THERMAL BOUNDARY CONDUCTANCE OF CARBON NANOFINS

XXIX Congresso UIT sulla Trasmissione del Calore
Torino, 20-22 Giugno 2011

THERMAL BOUNDARY CONDUCTANCE OF CARBON NANOFINS

Eliodoro Chiavazzo, Pietro Asinari

Department of Energetics, Politecnico di Torino, Corso Duca degli Abruzzi, 10129 Torino, Italy.
E-mail: eliodoro.chiavazzo@polito.it, pietro.asinari@polito.it

ABSTRACT

Nanofluids are suspensions of nanoparticles and fibers which have recently attracted much attention because of their superior thermal properties. Nevertheless, it was proven that, due to modest dispersion of nanoparticles, such high expectations often remain unmet. Introducing the notion of *nanofin*, a possible advancement was envisioned, where nanostructures with high aspect-ratio are sparsely attached to a solid surface and act as thermal bridges within the boundary layer (E. Chiavazzo, P. Asinari, *Nanoscale Research Letters*, 2011). In this context, we focus on single carbon nanotubes to enhance heat transfer between a surface and a fluid in contact with it. Thermal conductance at the interface between a single wall carbon nanotube (nanofin) and water molecules is assessed by means of both steady-state and transient numerical experiments. Numerical evidences suggest a pretty favorable thermal boundary conductance (order of 10^7 $\left[\mathrm{Wm^{-2}K^{-1}}\right]$) which makes carbon nanotubes potential candidates for constructing *nanofinned surfaces*.

BACKGROUND AND MOTIVATIONS

Nanofluids are suspensions of solid particles and/or fibers, which have recently become a subject of growing scientific interest because of reports of greatly enhanced thermal properties [1; 2]. Filler dispersed in a nanofluid is typically of nanometer size, and it has been shown that such nanoparticles are able to endow a base fluid with a much higher effective thermal conductivity than fluid alone [3].

In particular, carbon nanotubes (CNTs) have attracted great interest for nanofluid applications, because of the claims about their exceptionally high thermal conductivity [4]. However, recent experimental findings on CNTs report an *anomalously* wide range of enhancement values that continue to perplex the research community and remain unexplained [5].

Clearly, there are difficulties in the experimental measurements [6], but published results also reveal some underlaying technological problems. First of all, the CNTs show some bundling or the formation of aggregates originating from the fabrication step. Moreover, it seems reasonable that CNTs encounter *poor dispersibility* and suspension durability because of the aggregation and surface hydrophobicity of CNTs as a nanofluid filler. Therefore, the surface modification of CNTs or additional chemicals (surfactants) have been required for stable suspensions of CNTs, because of the polar characteristics of base fluid. In the case of surface modification of CNTs, water-dispersible CNTs have been extensively investigated for potential applications, such as biological uses, nanodevices, novel precursors for chemical reagents, and nanofluids [2].

It is reasonable to claim that, despite the great interest and intense research in this field, the results achieved so far cannot be considered really encouraging. Hence, toward the end of overcoming these problems, the notion of *thermal nanofins* was introduced [7], with an entirely different meaning with respect to standard terminology. By nanofins, we mean slender nano-structures, sparse enough not to interfere with the thermal boundary layer, but sufficiently rigid and conductive to allow for direct energy transfer between the wall and the bulk fluid, thus acting as thermal bridges. In this way, nanoparticles are used only where they are needed, namely, in the thermal boundary layer (or in the thermal laminar sub-layer, in case of turbulent flows, not discussed here), and this might finally unlock the enormous potential of the basic idea behind nanofluids.

This article investigates, by molecular mechanics based on force fields (MMFF), the thermal performance of nanofins made of single wall CNTs (SW-CNTs). The SW-CNTs were selected mainly because of time constraints of our parallel computational facilities. The following analysis can be split into two parts. First of all, the heat conductivity of SW-CNTs is estimated numerically (section "Heat conductivity of single-wall carbon nanotubes: detailed three dimensional models"). This first step is used for validation purposes in a vacuum and for comparison with results from literature. Next, the thermal boundary conductance between SW-CNT and water (for the sake of simplicity) is computed by two methods: the steady-state method (section "Steady-state simulations"), mimicking ideal cooling by a strong forced convection (thermostatted surrounding fluid), and the transient method (section "Transient simulations"), taking into account only atomistic interactions with the local fluid (defined by the simulation box). This strategy allows one to estimate a reasonable range for the thermal boundary conductance.

HEAT CONDUCTIVITY OF SW-CNTs: DETAILED THREE-DIMENSIONAL MODELS

In all simulations below, we have adopted the open-source molecular dynamics (MD) simulation package GROningen MAchine for Chemical Simulations (GROMACS) [8; 9; 10] to investigate the energy transport phenomena in three-dimensional SWNT obtained by a freely available structure generator (Tubegen) [11]. Three harmonic terms are used to describe the carbon–carbon-bonded interactions within the

Table 1. Parameters for carbon–carbon, carbon–water, and water–water interactions are chosen according to Guo et al. [12] and Walther et al. [13]

k^{b}_{ij} $\left[\mathrm{kJmol^{-1}nm^{-2}}\right]$	k^{θ}_{ijk} $\left[\mathrm{kJmol^{-1}}\right]$	k^{ϕ}_{ijkl} $\left[\mathrm{kJmol^{-1}}\right]$
47890	562.2	25.12
$\varepsilon_{\mathrm{CC}}$ $\left[\mathrm{kJ\cdot mol^{-1}}\right]$	σ_{CC} $\left[\mathring{A}\right]$	-
0.4396	3.851	-
$\varepsilon_{\mathrm{CO}}$ $\left[\mathrm{kJ\cdot mol^{-1}}\right]$	σ_{CO} $\left[\mathring{A}\right]$	-
0.3126	3.19	-
$\varepsilon_{\mathrm{OO}}$ $\left[\mathrm{kJ\cdot mol^{-1}}\right]$	σ_{OO} $\left[\mathring{A}\right]$	-
0.6502	3.166	-
q_{O} $[e]$	q_{H} $[e]$	-
-0.82	0.41	-

SWNT. That is, a bond stretching potential (between two covalently bonded carbon atoms i and j at a distance r_{ij}):

$$V_{\mathrm{b}}\left(r_{ij}\right)=\frac{1}{2}k^{b}_{ij}\left(r_{ij}-r^{0}_{ij}\right)^{2}, \tag{1}$$

a bending angle potential (between the two pairs of covalently bonded carbon atoms (i,j) and (j,k))

$$V_{\mathrm{a}}\left(\theta_{ijk}\right)=\frac{1}{2}k^{\theta}_{ijk}\left(\cos\theta_{ijk}-\cos\theta^{0}_{ijk}\right)^{2}, \tag{2}$$

and the Ryckaert-Bellemans potential for proper dihedral angles (for carbon atoms i, j, k and l)

$$V_{\mathrm{rb}}\left(\phi_{ijkl}\right)=\frac{1}{2}k^{\phi}_{ijkl}\left(1-\cos 2\phi_{ijkl}\right) \tag{3}$$

are considered in the following MD simulations. In this case, θ_{ijk} and ϕ_{ijkl} represent all the possible bending and torsion angles, respectively, while $r^{0}_{ij}=0.142\,\mathrm{nm}$ and $\theta^{0}_{ijk}=120^{\circ}$ are the reference geometry parameters for graphene. Non-bonded van der Waals interaction between two individual atoms i and j at a distance r_{ij} can be also included in the model by a Lennard-Jones (LJ) potential:

$$V_{\mathrm{nb}}=4\varepsilon_{CC}\left[\left(\frac{\sigma_{\mathrm{CC}}}{r_{ij}}\right)^{12}-\left(\frac{\sigma_{\mathrm{CC}}}{r_{ij}}\right)^{6}\right], \tag{4}$$

where the force constants k^{b}_{ij}, k^{θ}_{ijk} and k^{ϕ}_{ijkl} in (1), (2), and (3) and the parameters $(\sigma_{\mathrm{CC}},\varepsilon_{\mathrm{CC}})$ in (4) are chosen according to the Table 1 (see also [12; 13]). In reversible processes, differentials of heat $\mathrm{d}Q_{\mathrm{rev}}$ are linked to differentials of a state function, entropy, $\mathrm{d}s$ through temperature: $\mathrm{d}Q_{\mathrm{rev}}=T\,\mathrm{d}s$. Moreover, following Hoover [14; 15], entropy production of a Nosé-Hoover thermostat is proportional to the time average of the friction coefficient $\langle\xi\rangle$ through the Boltzmann constant k_{b}, and hence, once a steady-state temperature profile is established along the nanotube, the heat flux per unit area within the SWNT can be computed as

$$q=-\langle\xi\rangle\frac{N_{\mathrm{f}}k_{\mathrm{b}}T}{S_{\mathrm{A}}}, \tag{5}$$

where the cross section S_{A} is defined as $S_{\mathrm{A}}=2\pi rb$, with $b=0.34\,\mathrm{nm}$ denoting the van der Waals thickness (see also [16]). In this case, the use of formula (5) is particularly convenient since the quantity $\langle\xi\rangle$ can be readily extracted from the output files in GROMACS.

The measure of both the slopes of temperature profiles along the inner rings of SWNT in Figure 1 and the heat flux by (5) enables us to evaluate heat conductivity λ according to Fourier's law. Interestingly, in our simulations we can omit at will some of the interaction terms V_{b}, V_{a}, V_{rb}, and V_{nb}, and investigate how temperature profile and thermal conductivity λ are affected. It was found that potentials V_{b} and V_{a} are strictly needed to avoid a collapse of the nanotube. Results corresponding to several setups are reported in Figure 1. It is worth stressing that, for all simulations in a vacuum, non-bonded interactions V_{nb} proven to have a negligible effect on both the slope of temperature profile and heat flux at steady state. On the contrary, the torsion potential V_{rb} does have impact on the temperature profile while no significant effect on the heat flux was noticed: as a consequence, in the latter case, thermal conductivity shows a significant dependence on V_{rb}. More specifically, the higher the torsion rigidity the flatter the temperature profile. Depending on the CNT length (and total number of atoms), computations were carried out for 4 ns up to 6 ns to reach a steady state of the above non-equilibrium molecular dynamics (NEMD) simulations. Finally, temperature values of the end-points of CNTs (see Figures 1) were chosen following others [16; 17].

THERMAL BOUNDARY CONDUCTANCE OF A CARBON NANOFIN IN WATER

Steady-state simulations

In this section, we investigate on the heat transfer between a carbon nanotube and a surrounding fluid (water). The latter represents a first step toward a detailed study of a batch of single CNTs (or small bundles) utilized as *carbon nanofins* to enhance the heat transfer of a surface when transversally attached to it. To this end, and limited by the power of our current computational facilities, we consider a $(5,5)$ SWNT (with a length $L\leq 14\,\mathrm{nm}$) placed in a box filled with water (typical setup is shown in Figure 2). SWNT end temperatures are set at a fixed temperature $T_{\mathrm{hot}}=360\,\mathrm{K}$, while the solvent is kept at $T_{\mathrm{w}}=300\,\mathrm{K}$. The carbon–water interaction is taken into account by means of a Lennard-Jones potential between the carbon and oxygen atoms with a parameterization ($\varepsilon_{\mathrm{CO}}$, σ_{CO}) reported in Table 1. Moreover, non-bonded interactions between the water molecules consist of both a Lennard-Jones term between oxygen atoms (with $\varepsilon_{\mathrm{OO}}$, σ_{OO} from Table 1) and a Coulomb potential:

$$V_{\mathrm{c}}\left(r_{ij}\right)=\frac{1}{4\pi\varepsilon_{0}}\frac{q_{i}q_{j}}{r_{ij}}, \tag{6}$$

where ε_{0} is the permittivity in a vacuum, while q_i and q_j are the partial charges with $q_{\mathrm{O}}=-0.82\,\mathrm{e}$ and $q_{\mathrm{H}}=0.41\,\mathrm{e}$ (see also [13]).

We notice that, the latter is a classical problem of heat transfer, where a single fin (heated at the ends) is immersed in a fluid maintained at a fixed temperature. This system can be conveniently treated using a continuous approach under the assumptions of homogeneous material, constant cross section S, and one-dimensionality (no temperature gradients within a given cross section) [18]. In this case, both temperature field and heat flux only depend on the spatial coordinate x (varying along the axial direction), and the analytic solution of the energy conservation equation yields, at the steady state, the following relationship:

$$\tilde{T}(x) = Me^{-mx} + Ne^{mx}, \tag{7}$$

where $\tilde{T}(x) = T(x) - T_{\mathrm{w}}$ denotes the difference between the local temperature at an arbitrary position x and the fixed temperature T_{w} of a surrounding fluid. Let α and C be the thermal boundary conductance and the perimeter of the fin cross sections, respectively, m be linked to geometry, and material properties as follows:

$$m = \sqrt{\frac{\alpha_{\mathrm{st}} C}{\lambda S}}, \tag{8}$$

whereas the two parameters M and N are dictated by the boundary conditions, $T(0) = T(L) = T_{\mathrm{hot}}$ (or equivalently, due to symmetry, zero flux condition: $\mathrm{d}T/\mathrm{d}x(L/2) = 0$), namely:

$$M = \tilde{T}(0)\frac{e^{mL/2}}{e^{mL/2} + e^{-mL/2}}, \quad N = \tilde{T}(0)\frac{e^{-mL/2}}{e^{mL/2} + e^{-mL/2}}. \tag{9}$$

Thus, the analytic solution (7) takes a more explicit form:

$$\tilde{T}(x) = \tilde{T}(0)\frac{\cosh\left[m\left(L/2 - x\right)\right]}{\cosh\left(mL/2\right)}, \tag{10}$$

whereas the heat flux at one end of the fin reads:

$$q_0 = m\lambda S\tilde{T}\left(0\right)\tanh\left(mL/2\right). \tag{11}$$

In the setup illustrated in Figure 2, periodic boundary conditions are applied in all directions, and simulations are carried out with a fixed time step $\mathrm{d}t = 1\,\mathrm{fs}$ upon energy minimization. First of all, the whole system is led to thermal equilibrium at $T = 300$ by Nosé-Hoover thermostatting implemented for 0.8 ns with a relaxation time $\tau_{\mathrm{T}} = 0.1\,\mathrm{ns}$. Next, the simulation is continued for 15 ns where Nosé-Hoover temperature coupling is applied only at the tips of the nanofin (here, the outermost 16 carbon atom rings at each end) with $T_{\mathrm{hot}} = 360\,\mathrm{K}$, and in water with $T_{\mathrm{w}} = 300\,\mathrm{K}$ until, at the steady state, the temperature profile in Figure 3 is developed. Moreover, pressure is set to 1 bar by Parrinello-Rahman barostat during both thermal equilibration and subsequent non-equilibrium computation. We notice that the above MD results are in a good agreement with the continuous model for single fins if $mL/2 = 0.28$ (see also Figure 3). Hence, this enables us to estimate the thermal boundary conductance α_{st} between SWNT and water with the help of Equation (8):

$$\alpha_{\mathrm{st}} = \frac{m^2\lambda S}{C}. \tag{12}$$

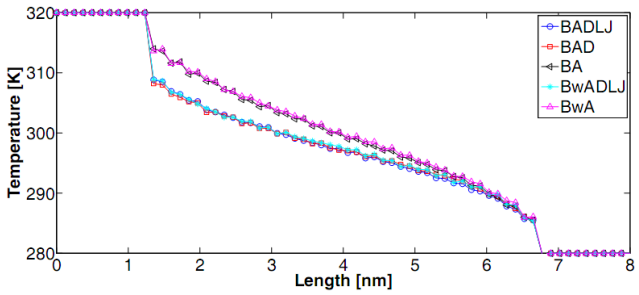

Figure 1. Temperature profiles along a SWCNT at steady state. Several setups have been tested where some of the interaction potentials (1), (2), (3), and (4) are omitted. BADLJ: V_{b}, V_{an}, V_{rb}, and V_{nb} are considered. BAD: V_{b}, V_{an}, V_{rb} are considered. BA: V_{b} and V_{an} are considered. Bw denotes that V_{b} is computed with a smaller force constant $k_{ij}^{\mathrm{b}} = 42000\,\mathrm{kJ}\cdot\mathrm{mol}^{-1}\cdot\mathrm{nm}^{-2}$ according to [23].

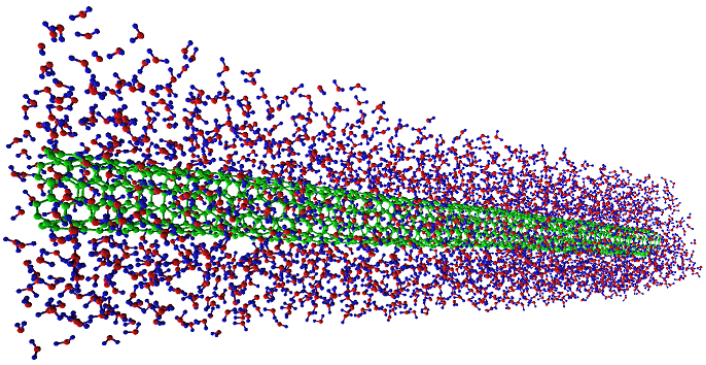

Figure 2. A $(5,5)$ SWNT (green) is surrounded by water molecules (blue, red). Nosé-Hoover thermostats with temperature $T_{\mathrm{hot}} = 360\,\mathrm{K}$ are coupled to the nanotube tips, while water is kept at a fixed temperature $T_{\mathrm{w}} = 300\,\mathrm{K}$. After a sufficiently long time (here 15 ns), a steady-state condition is reached. MD simulation results (in terms of both temperature profile and heat flux) are consistent with a continuous one-dimensional model as described by Equations (10) and (11). Image obtained using VEGA ZZ [24].

The thermal conductivity λ has been independently computed by means of the technique illustrated in the sections above for the SWNT alone in a vacuum. Results for a nanofin whose length is 14 nm are reported in Table 2. We stress that heat flux computed by time averaging of the Nosé-Hoover parameter ξ (see Equation (5)) is also in excellent agreement with the value predicted by the continuous model through Equation (11). For instance, with the above choice $mL/2 = 0.28$, for $(5,5)$ SWNT with $L = 10\,\mathrm{nm}$, $L_{\mathrm{NH}} = 2\,\mathrm{nm}$ in a box $5\times5\times14\,\mathrm{nm}^3$ we have: $-\langle\xi\rangle N_{\mathrm{f}} k_{\mathrm{b}} T = 3.11\times10^{-8}\,\mathrm{W}$ while

$$q_0 = m\lambda S\tilde{T}\left(0\right)\tanh\left(mL/2\right) = 3.14\times10^{-8}\,\mathrm{W}. \tag{13}$$

We stress that L_{NH} is the axial length of the outermost carbon atom rings coupled to a thermostat at each end of a nanotube.

Transient simulations

The value of thermal boundary conductance between water and a SW-CNT has been assessed by transient simulations as well. Results by the latter methodology are denoted as α_{tr} to distinguish them from the same quantities (α_{st}) in the above sec-

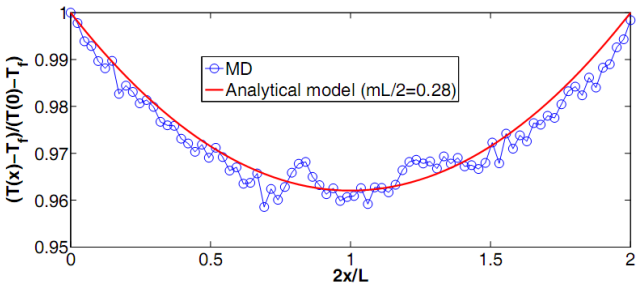

Figure 3. Steady state molecular dynamics (MD) simulations. Dimensionless temperature computed by MD (symbols) versus temperature profile predicted by continuous model (line), Eq. (10). Best fitting is achieved by choosing $mL/2 = 0.28$. Case with computational box $2.5 \times 2.5 \times 14[nm^3]$.

tion. In this study, the nanotube was initially heated to a predetermined temperature $T_{\rm hot}$ while water was kept at $T_{\rm w} < T_{\rm hot}$ (using in both cases Nosé-Hoover thermostatting for 0.6 ns). Next, an NVE MD (ensemble where number of particle N, system volume V and energy E are conserved) were performed, where the entire system (SWNT plus water) was allowed to relax without any temperature and pressure coupling. Under the assumption of a uniform temperature field $T_{\rm CNT}(t)$ within the nanotube at any time instant t (i.e., Biot number Bi < 0.1), the above phenomenon can be modeled by an exponential decay of the temperature difference $(T_{\rm CNT} - T_{\rm w})$ in time, where the time constant $\tau_{\rm d}$ depends on the nanotube heat capacity $c_{\rm T}$ and the thermal heat conductance $\alpha_{\rm tr}$ at the nanotube–water interface as follows (see Figure 4):

$$\tau_{\rm d} = \frac{c_{\rm T}}{\alpha_{\rm tr}}. \qquad (14)$$

In our computations, based on [19], we considered the heat capacity per unit area of an atomic layer of graphite $c_{\rm T} = 5.6 \times 10^{-4}\,({\rm J \cdot m^{-2} \cdot K^{-1}})$.

The values of $\tau_{\rm d}$ and $\alpha_{\rm tr}$ have been evaluated in different setups, and results are reported in the Table 2. Numerical computations do predict pretty high thermal conductance at the interface (order of $10^7\,{\rm W \cdot m^{-2} \cdot K^{-1}}$) with a slight tendency to increase with both the tube length and diameter. It is worth stressing that values for thermal boundary conductance obtained in this study are consistent with both experimental and numerical results found by others for SW-CNTs within liquids [19; 21]. However, since the order of magnitude of these results is extremely higher than that involved in macroscopic applications, it may appear as an artifact. Actually, it is quite simple to realize that continuum-based models diverge in case of nanometer dimensions, because of the effects of singularity. Hence, continuum-based predictions may lead to even higher thermal conductances, and they are not even upper bounded, which is clearly unphysical. For example, let us consider the ideal case of a circular cylinder (with diameter D and length L) centered in a square solid of equal length, as reported in Table 3.12 of [20]. The value of thermal boundary conductance can be put into relation with the heat conduction shape factor (CSF) $S_{\rm f}$ as follows:

$$\alpha_{\rm csf} = \frac{S_{\rm f}\lambda_{\rm w}}{\pi D L}, \qquad (15)$$

Table 2. Summary of the results of the presented study. SW-CNTs with chirality $(3,3)$, $(5,5)$, and $(15,0)$ are considered.

Chirality	Length $[nm]$	α_{st} $[Wm^{-2}K^{-1}]$	α_{tr} $[Wm^{-2}K^{-1}]$
$(5,5)$	14	5.18×10^7	-
$(5,5)$	14	-	1.70×10^7
$(15,0)$	4.7	-	1.60×10^7
$(3,3)$	3.7	-	8.90×10^6

where

$$S_{\rm f} = \frac{2\pi L}{\ln(1.08 w/D)}, \qquad (16)$$

and $\lambda_{\rm w}$ is the thermal conductivity of the medium, while the square box has dimensions $w \times w \times L$. Let us consider the following example, corresponding to the first row in Table 2. Assuming $\lambda_{\rm w} = 0.58\ ({\rm W \cdot m^{-1} \cdot K^{-1}})$, $D = 0.68$ nm, $w = 4$ nm, it yields $\alpha_{\rm csf} = 9.2 \times 10^8\,{\rm W\,m^{-2}\,K^{-1}}$.

The analytic results are even larger than those obtained by the steady-state simulation (usually larger than those obtained by the transient method). Moreover, the continuum-based formula prescribes that thermal conductance (weakly) diverges by reducing the cylinder diameter. On the contrary, MD simulations is in line with the expectation of a bounded thermal boundary conductance. In fact, in agreement with others [21], we even observe a slight decrease with the tube diameter. We point out that neither the steady-state method nor the transient method fully reproduce the setup described by the analytic formula (15). In fact, in the steady-state method, the entire water bath is thermostatted (while in the analytic formula, only the water boundaries are thermostatted) and, in the transient method, the water temperature changes in time (while the analytic formula is derived under steady-state condition). Nevertheless, from the technological point of view, the above results are in line with the basic idea that high aspect-ratio nanostructures (such as CNTs) are suitable candidates for implementing the above idea of *nanofin*, and thus can be utilized for exploiting advantageous heat boundary conductances.

CONCLUSIONS

In this study, we first investigated the thermal conductivity of SW-CNTs by means of classical non-equilibrium MD. Next, based on the latter results, we have focused on the boundary conductance and thermal efficiency of SW-CNTs used as nanofins within water. More specifically, toward the end of computing the boundary conductance α, two different approaches have been implemented. First, $\alpha = \alpha_{\rm st}$ was estimated through a fitting procedure of results by steady-state MD simulations and a simple one-dimensional continuous model. Second, cooling of SWNT (at $T_{\rm CNT}$) within water (at $T_{\rm w}$) was accomplished by NVE simulations. In the latter case, the time constant $\tau_{\rm d}$ of the temperature difference $(T_{\rm CNT} - T_{\rm w})$ dynamics enables us to compute $\alpha = \alpha_{\rm tr}$. Numerical computations do predict pretty high thermal conductance at the interface (order of $10^7\,{\rm W \cdot m^{-2} \cdot K^{-1}}$), which indeed makes CNTs ideal candidates for constructing nanofins. We should stress that, consistently with our results $\alpha_{\rm st} > \alpha_{\rm tr}$, it is reasonable to expect that

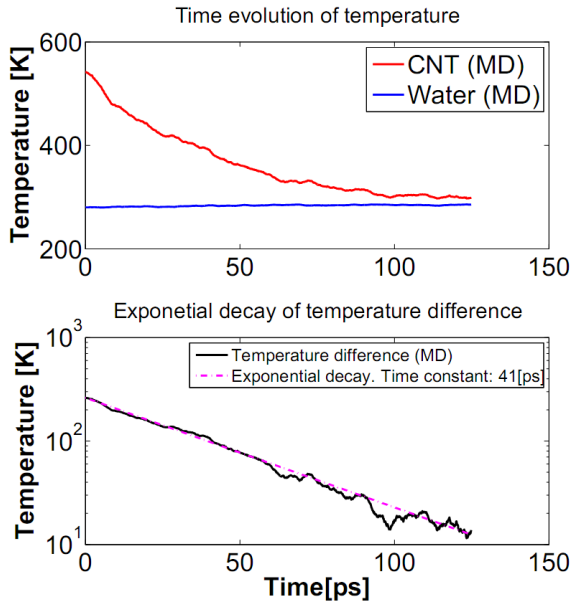

Figure 4. Transient simulations: temperature evolution as predicted by NVE molecular dynamics. Best fitting of exponential decay of the temperature difference $T_{\mathrm{CNT}} - T_{\mathrm{w}}$ is achieved by choosing $\tau_{\mathrm{d}} = 41\,\mathrm{ps}$.

α_{st} represents the upper limit for the thermal boundary conductance, because (in steady-state simulations) water is forced by the thermostat to the lowest temperature at any time and any position in the computational box. Finally, it is worthwhile stressing that, following the suggestion in [22], all the results of this study can be generalized to different fluids using standard non-dimensionalization techniques, upon a substitution of the parameterization ($\varepsilon_{\mathrm{CO}}$, σ_{CO}) representing a different Lennard-Jones interaction between SWNT and fluid molecules.

ACKNOWLEDGMENT

The above research has received funding from the European Community Seventh Framework Program (FP7 2007-2013) under grant agreement N. 227407-Thermonano. The authors owe their appreciation to Mr. Marco Giardino for his kind assistance whenever the authors had difficulites with computational facilities. The authors also thank Dr. Andrea Minoia and Dr. Thomas Moore for the fruitful discussions with them on the usage of GROMACS in simulating carbon nanotubes. The authors acknowledge also the inspiring discussions with Dr. Jean-Antoine Gruss (CEA DTS/LETH, France) about CNT-based nanofluids.

NOMENCLATURE

V_b, V_a, V_{rb} Interaction potentials due to covalent bonds
V_{nb} LJ interaction potential
V_c Coulomb potential
k^b_{ij} Force constant
k^θ_{ijk} Angular force constant
k^ϕ_{ijkl} Dihedral force constant
r_i Distance between atoms i and j
c_T Heat capacity
q Heat flux per unit area
N_f Number of degrees of freedom
k_b Boltzmann constant
T Temperature
$\tilde{T}$ Temperature difference
S_A Cross section
S_f Shape factor
w Edge of the computational box
D Diameter
q_O, q_H Partial charges
C Perimeter of the nanofin cross section
L Length of the nanofin
θ_{ijk} Bending angle
ϕ_{ijkl} Torsion angle
ε_{CC}, σ_{CC} LJ parameterization for carbon-carbon interaction
ε_{CO}, σ_{CO} LJ parameterization for carbon-oxygen interaction
ε_{OO}, σ_{OO} LJ parameterization for oxygen-oxygen interaction
ξ Nosé-Hoover friction coefficient
ε_0 Permittivity in a vacuum
τ_d Time constant
τ_T Relaxation time
λ Thermal conductivity
α_{st}, α_{tr}, α_{csf} Thermal boundary conductance

REFERENCES

[1] Wang L, Fan J: **Nanofluids research: key issues**. *Nanoscale Res Lett* 2010, **5**:1241-1252.
[2] Lee K, Yoon S, Jang J: **Carbon nanofibers: a novel nanofiller for nanofluid applications**. *Small* 2007, **3**:1209-1213.
[3] Hwang Y, Ahn Y, Shin H, Lee C, Kim G, Park H, Lee J: **Investigation on characteristics of thermal conductivity enhancement of nanofluids**. *Curr Appl Phys* 2005, **6**:1068-1071.
[4] Berber S, Kwon YK, Tomanek D: **Unusually high thermal conductivity of carbon nanotubes**. *Phys Rev Lett* 2000, **84**:4613-4616.
[5] Venkata Sastry N, Bhunia A, Sundararajan T, Das S: **Predicting the effective thermal conductivity of carbon nanotube based nanofluids**. *Nanotechnology* 2008, **19**:055704.
[6] Choi T, Maneshian M, Kang B, Chang W, Han C, Poulikakos D: **Measurement of the thermal conductivity of a water-based single-wall carbon nanotube colloidal suspension with a modified 3-omega method**. *Nanotechnology* 2009, **21**:315706.
[7] Chiavazzo E, Asinari P: **Enhancing surface heat transfer by carbon nanofins: towards an alternative to nanofluids?** *Nanoscale Research Letters* 2011, **6**:249.
[8] Berendsen H, van der Spoel D, van Drunen R: **GROMACS: a message-passing parallel molecular dynamics implementation**. *Comp Phys Commun* 1995, **91**:43-56.
[9] Lindahl E, Hess B, van der Spoel D: **Gromacs 3.0: a package for molecular simulation and trajectory analysis**. *J Mol Mod* 2001, **7**:306-317.
[10] **GROMACS fast flexible free** `http://www.gromacs.org/`.
[11] **Frey JT, Doren DJ, University of Delaware, Newark DE, 2005. TubeGen 3.3** `http://turin.nss.udel.edu/research/tubegenonline.html`.
[12] Guo Y, Karasawa N, Goddard W: **Prediction of fullerene packing in C_{60} and C_{70} crystals**. *Nature* 1991, **351**:464-467.
[13] Walther JH, Jaffe R, Halicioglu T, Koumoutsakos P: **Carbon nanotubes in water: structural characteristics and**

energetics. *J Phys Chem B* 2001, **105**:9980-9987.

[14] Hoover WG, Posch HA: **Second-law irreversibility and phase-space dimensionality loss from time-reversible nonequilibrium steady-state Lyapunov spectra**. *Phys Rev E* 1994, **49**:1913-1920.

[15] Hoover WG, Hoover CG: **Links between microscopic and macroscopic fluid mechanics**. *Mol Phys* 2003, **101**:1559-1573.

[16] Shelly R, Toprak K, Bayazitoglu Y: **Nose-Hoover thermostat length effect on thermal conductivity of single wall carbon nanotubes**. *Int J Heat Mass Transf* 2010, **53**:5884-5887.

[17] Zhong H, Lukes J: **Interfacial thermal resistance between carbon nanotubes: molecular dynamics simulations and analytical thermal modeling**. *Phys Rev B* 2006, **74**:125403.

[18] Kreith F, Bohn MS: *Principles of Heat Transfer*. Brooks/Cole 2001.

[19] Huxtable S T, Cahill D G, Shenogin S, Xue L, Ozisik R, Barone P, Usrey M, Strano M S, Siddons G, Shim M, Keblinski P: **Interfacial heat flow in carbon nanotube suspensions**. *Nat Mater* 2003, **2**:731-734.

[20] Bejan A, Kraus A: *Heat Transfer Handbook*. Hoboken: Wiley; 2003.

[21] Shenogin S, Xue L, Ozisik R, Keblinski P, Cahill D: **Role of thermal boundary resistance on the heat flow in carbon-nanotube composites**. *J Appl Phys* 2004, **95**:8136-8144.

[22] Zhong H, Lukes JR: **Interfacial thermal resistance between carbon nanotubes: molecular dynamics simulations and analytical thermal modeling**. *Phys Rev B* 2006, **74**:125403.

[23] Brenner DW, Shenderova OA, Harrison JA, Stuart SJ, Boris N, Sinnott SB: **A second-generation reactive empirical bond order (REBO) potential energy expression for hydrocarbons**. *J Phys Condens Matter* 2002, **14**:783-802.

[24] Pedretti A, Villa L, Vistoli G: **VEGA: A versatile program to convert, handle and visualize molecular structure on windows-based PCs**. *J Mol Graph* 2002, **21**:47-49.